Evaluating uncertainties in electrochemical impedance spectra of solid oxide fuel cells

Luka Žnidarič^{a,b,*}, Gjorgji Nusev^{a,b}, Bertrand Morel^c, Julie Mougin^c, Đani Juričić^a, Pavle Boškoski^a

^a Jožef Stefan Institute, Jamova cesta 39, SI-1000 Ljubljana, Slovenia ^b Jožef Stefan International Postgraduate School, Jamova cesta 39, SI-1000 Ljubljana, Slovenia ^c Laboratoire des Technologies Hydrogèn Commissariat à l'énergie atomique et aux énergies alternatives - CEA, CEA/LITEN/DTBH/STHB/LTH 17 rue des Martyrs - 38054 GRENOBLE CEDEX 9, France

Abstract

Electrochemical impedance spectroscopy (EIS) is a widely used tool for characterization of fuel cells and electrochemical conversion systems in general. When applied to the on-line monitoring in context of infield applications, the disturbances, drifts and sensor noise may cause severe distortions in the evaluated spectra, especially in the low-frequency part. Failure to account for the random effects can implicate difficulties in interpreting the spectra and misleading diagnostic reasoning. In the literature, this fact has been largely ignored. In this paper, we propose a computationally efficient approach to the quantification of the spectral uncertainty by quantifying the uncertainty of the equivalent circuit model (ECM) by means of the variational Bayes approach (VB) approach. To assess the quality of the VB posterior estimates, we compare the results of VB approach with those obtained with the Markov chain Monte Carlo (MCMC) algorithm. Namely, MCMC algorithm is expected to return accurate posterior distributions, while VB approach provides the approximative distributions. By using simulated and real data we show that VB approach generates approximations, which although slightly over-optimistic, are still pretty close to the more realistic MCMC estimates. A great advantage of the VB method for online monitoring is low computational load, which is several orders of magnitude lighter than that of MCMC. The performance of VB algorithm is demonstrated on a case of ECM parameters estimation in a 6 cell solid-oxide fuel cell (SOFC) stack. The complete numerical implementation for recreating the results can be found at https://repo.ijs.si/ lznidaric/variational-bayes-supplementary-material.

Keywords: Variational Bayes, Monte Carlo, Solid-oxide fuel cells, Fractional-order systems

1. Introduction

Currently available tools for characterising electrochemical energy systems predominantly rely on Nyquist curves obtained through electrochemical impedance spectroscopy (EIS) [1]. Conceptually simple and well

Email address: luka.znidaric@ijs.si (Luka Žnidarič)

^{*}Corresponding author.

understood, EIS analysis has proven to be a standard tool for characterising the health condition of cells and stacks. Correct evaluation of the EIS characteristic is subject to several requirements.

First, the perturbation signal must have low amplitude in order to not excite the nonlinear modes of the cells. If the amplitudes are too small, there is a risk that the noise-to-signal ratio will decrease, which will be reflected in an increased variance of the EIS estimates. Second, the cells should operate in stationary, stable, and repeatable test conditions. This is mandatory for a correct evaluation of the EIS curves. This means that the internal conditions should remain constant during the measurement and that no external perturbations should corrupt the measurements. Under well-controlled laboratory conditions, the perturbations are kept under control, which usually results in smooth Nyquist curves. This is the only possible way of obtaining data that can be validly compared for potential discrepancy used as an indicatior of a fault or degradation. Third, to obtain comparable results, measurements on a cell or stack should be performed at the same operating point. The above requirements are not easily met in applications outside laboratories.

In the in-field operation, it is not possible to guarantee complete control over fluctuations in the balance of plant (BoP) and system environment. For example, drift and noise in flows and temperatures can affect the low-frequency part of the Nyquist curve. Indeed, non-stationary external conditions such as temperature or load variations are unavoidable in real applications and can therefore contribute to non-smooth results. Increased noise in current and voltage measurements can also contribute to the non-smooth EIS estimates. In addition, unsafe operating conditions, such as increased fuel utilization, can cause increased variance in the low-frequency portion of the spectra due to local fuel starvation problems, which then affect the voltage variance.

How to handle the effects of the uncontrolled random perturbations on the EIS evaluation and cell characterization is the problem addressed in this paper. A strong motivation for the work stems from several of our own practical implementations as well as a large number of evidences found in the literature, e.g. [2, 3]. For better illustration, Figure 1 shows the evaluated EIS curves obtained from successive measurements performed on a solid-oxide fuel cell (SOFC) stack operating in laboratory conditions and on in-field application. It appears that a combination of the above factors results in a high spread of EIS values at low frequencies. Note that the perturbations do not significantly affect the high frequency range arcs in the EIS curve.

It seems that this problem has not yet been systematically addressed, at least in what concerns SOFC domain. With the increasing need for automated condition monitoring, robust solutions are mandatory to ensure reliable and stable diagnosis. This is important since the mitigation actions are undertaken from the diagnostic results. Unreliable EIS evaluations can result in misleading diagnosis and countermeasures that can even worsen the condition of the cell or stack.

An idea of how to deal with the problem in SOFCs was recently proposed in articles [4, 5]. The author performs inference on the equivalent circuit modes based on a combination of EIS data smoothing and EIS averaging. Instead of using a single EIS measurement, the data from several consecutive EIS measurements

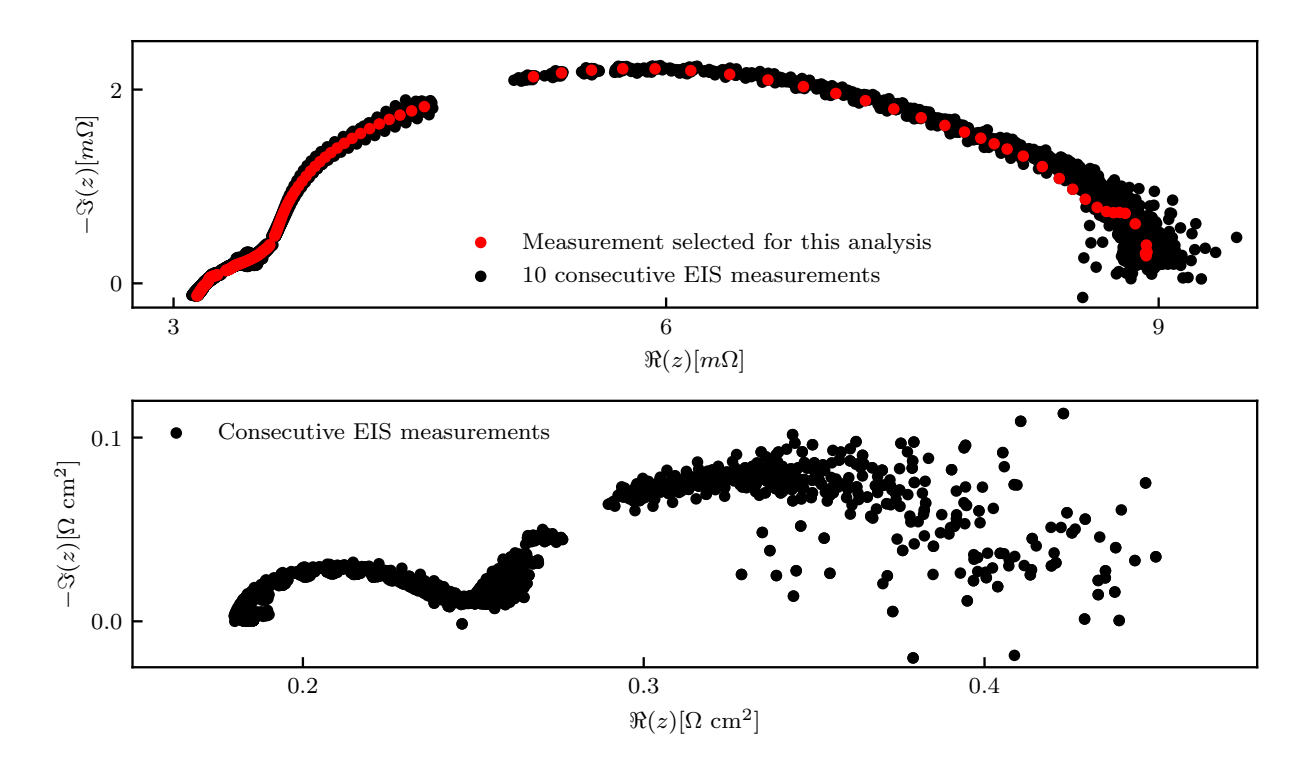


Figure 1: Evaluated EIS characteristics in laboratory conditions (above) and during an in-field application (below).

are averaged to reduce the spread of the estimates in the low-frequency region. This solution, while simple, requires a certain number of measurements spanned on a time window to reliably assess the change in the EIS characteristic.

In this paper, we propose a novel approach, not pursued before, which is able to account for the influence of perturbations on the evaluated EIS characteristic and the equivalent circuit model by a statistical approach. Properly quantified uncertainties lead to diagnostic solutions that, rather than making a fault statement in clear yes/no categories, suggest the probability that a particular fault is present [6]. This is essential for a cautious and more reliable diagnosis of SOFCs, which can be additionally enhanced with the operator's prior knowledge.

In the area of electrochemical energy conversion systems, there have been only limited attempts to analyze the stochastic nature of the parameters. The parameters of the ECM model are usually obtained by constrained nonlinear optimization, c.f. [7, 8], resulting in the parameter vector $\boldsymbol{\theta}^*$ which minimizes some criterion (loss of fit) function $J(\boldsymbol{\theta})$. The simplest and most straightforward approach to evaluate the uncertainty is to locally approximate the criterion function with the second-order function $J(\boldsymbol{\theta}) \approx J(\boldsymbol{\theta}^*) + (\boldsymbol{\theta} - \boldsymbol{\theta}^*)' \boldsymbol{\Sigma}(\boldsymbol{\theta} - \boldsymbol{\theta}^*)$. The uncertainty region is approximated by the ellipsoid defined by the Hessian matrix $\boldsymbol{\Sigma}$. The problem with this approach is that the approximation is rather rough and might suggest a misleading uncertainty region [9]. To obtain a realistic estimate of the uncertainty of the parameters,

more elaborated approaches should be applied. Of the available methods, the Markov chain Monte Carlo (MCMC) simulation [10] is the most accurate for fractional system parameter estimation. The biggest problem with this approach is the overwhelming computational time, which increases rapidly with the number of unknown parameters. For potential applications in the field, a computationally less excessive but still sufficiently accurate method is welcome.

One approach that offers a way to circumvent the issues imposed by MCMC is the variational Bayes approach (VB) [11]. Unlike the Monte Carlo approach that results in the "true" posterior distribution, the VB provides the closest approximation of the posterior distribution using the probability distribution functions from the exponential family as building blocks. Consequently, instead of solving the typically intractable evidence integral in Bayesian theorem, the posterior distribution in VB is found through optimisation. The result contains inherent bias, but this is a small price to pay considering the impressive computational efficiency of the approach even for multidimensional cases. VB has been successfully applied in various areas, such as Gaussiaxn process modeling [12, 13], deep generative models [14], compressed sensing [15, 16], Hidden Markov models [17, 18], reinforcement learning and control [19]. VB is also applicable to energy management problems [20–24].

In this paper we want to analyse the nature and shape of the uncertainty regions for our parameters and compare the results of the computationally feasible VB approach and the well established MCMC. To the best of the authors' knowledge, the first attempt to study the uncertainty of equivalent circuit model (ECM) estimates has been done in [25]. This work provided the first report on the marginal probability distribution functions of the ECM parameters under nominal operating conditions. However, the method is practically infeasible for online monitoring since it takes several hours even with a strong HPC infrastructure. It takes about 25 hours of computational time to get quality posterior distributions. What we suggest below is to approximate the true posterior probability density function with a closed form distribution that best captures the nature of the true posterior. The benefits of having the uncertainties of the model parameters explained in the closed form are twofold. First, we get a useful indicator of the quality of the selected ECM model structure and the quality of the experimental data leading to the model. Second, it becomes possible to rather easily employ statistical reasoning tools for detecting changes in the posterior of the ECM parameters and thus the deterioration of the system behaviour. This is therefore the first attempt to show the applicability of VB in the field of electrochemistry.

The structure of the paper is as follows. A brief introduction to the MCMC and VB approach is given in section 2. The performance of the method in terms of computational efficiency and accuracy is first demonstrated on a simulated ECM in section 3. Finally, the VB is applied to the identification of ECM parameters based on data obtained on a SOFC in section 4. The complete numerical implementation for

¹HPC Meister, capability: 244 TFLOPs

recreating the results is provided as a supplementary material in Appendix A.

2. Methodology

The presented inference approach arises from the Bayes rule (1). Let us assume a set of measured data \mathbf{x} generated by a system with the parameters $\boldsymbol{\theta}$. The Bayes' rule (1) provides a link between the posterior distribution (the updated information about the model parameters) based on the prior probability of the model parameters $p(\boldsymbol{\theta})$ and the likelihood that the observations \mathbf{x} are generated by a model with the parameters $\boldsymbol{\theta}$

$$\underbrace{p(\boldsymbol{\theta}|\mathbf{x})}_{\text{Posterior}} = \underbrace{\frac{p(\mathbf{x}|\boldsymbol{\theta})}{p(\boldsymbol{\theta})}}_{\text{Evidence}} \underbrace{\frac{p(\mathbf{x})}{p(\boldsymbol{\theta})}}_{\text{Evidence}} \tag{1}$$

The likelihood can be calculated from the model and the prior is specified as a design input. The normalisation factor (evidence) is the following integral:

$$p(\mathbf{x}) = \int_{\boldsymbol{\theta}} p(\mathbf{x}|\boldsymbol{\theta}) p(\boldsymbol{\theta}) d\boldsymbol{\theta}. \tag{2}$$

For general multidimensional distributions the integral (2) becomes intractable. Consequently, getting the posterior in (1) becomes infeasible, hence the need for the approximate approaches.

2.1. Markov Chain Monte Carlo

MCMC algorithm is a ubiquitous method for solving integration problems in various areas, e.g. statistics, physics and econometrics. Central in the approach is the way of taking samples, say a set of N samples $\boldsymbol{\theta}^{(i)} \in \mathbb{R}^m$, i = 1, ..., N, from a target density $p(\boldsymbol{\theta})$. Using these N samples, we can approximate $p(\boldsymbol{\theta})$, by calculating the empirical point-mass function

$$p_N(\boldsymbol{\theta}) = \frac{1}{N} \sum_{i=1}^N \delta_{\boldsymbol{\theta}^{(i)}}(\boldsymbol{\theta}),$$

where $\boldsymbol{\theta}^{(i)}$ is the i^{th} sample in our set θ and $\delta_{\boldsymbol{\theta}^{(i)}}$ is its delta-Dirac mass.

In our case we used MCMC with No-U-Turn sampling (NUTS) [26], implemented in Python with the PyMC3 [27] library. NUTS sampling is an extension of the well known Hamiltonian Monte Carlo algorithm (HMC) [28]. HMC tends to be sensitive to the required user inputs. This is mostly avoided since the NUTS algorithm stops automatically when it starts retracing its steps. Additionally authors of the NUTS additionally developed a method for automatic adaptation of the step size so that the sampler needs minimal user-defined parameters on entry. We let the algorithm run for 300.000 iterations, which proved sufficient to guarantee convergence.

2.2. Variational Bayes approach

Using MCMC methods for solving (2) can produce results very close to the true posterior distribution. However, for the multidimensional cases, the computational load and sheer number of samples required for obtaining proper estimate of the posterior blows up. One solution to this problem is to find a sufficiently close approximation of the posterior with the significantly lower computational load.

The main idea of the VB is finding a candidate distribution $q_{\lambda}(\boldsymbol{\theta})$ (parameterized with the latent hyperparameters $\lambda \in \mathbb{R}^{\nu}$), that is a sufficiently close approximation of the true posterior $p(\boldsymbol{\theta}|\mathbf{x})$. The distribution $q_{\lambda}(\boldsymbol{\theta})$ is usually referred to as the variational distribution. The variational distribution is typically selected from the mean-field variational family [29]. This means that one can assume independence among the latent variables of the variational distribution.

A variational distribution that is the best fit for the true posterior can be obtained by minimizing the Kullback-Leibler (KL) divergence [29], which can be re-arranged as follows:

$$KL(q_{\lambda}(\boldsymbol{\theta})||p(\boldsymbol{\theta}|\mathbf{x})) = \mathbb{E}_{q} \left[\log \frac{q_{\lambda}(\boldsymbol{\theta})}{p(\boldsymbol{\theta}|\mathbf{x})} \right]$$

$$= \mathbb{E}_{q} [\log q_{\lambda}(\boldsymbol{\theta})] - \mathbb{E}_{q} [\log p(\boldsymbol{\theta}|\mathbf{x})]$$

$$= \mathbb{E}_{q} [\log q_{\lambda}(\boldsymbol{\theta})] - \mathbb{E}_{q} [\log p(\mathbf{x}, \boldsymbol{\theta}) - \log p(\mathbf{x})]$$

$$= \mathbb{E}_{q} [\log q_{\lambda}(\boldsymbol{\theta})] - \mathbb{E}_{q} [\log p(\boldsymbol{\theta}, \mathbf{x})] + \log p(\mathbf{x})$$

$$= -(\mathbb{E}_{q} [\log p(\boldsymbol{\theta}, \mathbf{x})] - \mathbb{E}_{q} [\log q_{\lambda}(\boldsymbol{\theta})] + \log p(\mathbf{x})$$

$$= -(\mathbb{E}_{q} [\log p(\mathbf{x}|\boldsymbol{\theta})p(\boldsymbol{\theta})] - \mathbb{E}_{q} [\log q_{\lambda}(\boldsymbol{\theta})]) + \log p(\mathbf{x})$$

$$= -(\mathbb{E}_{q} [\log p(\mathbf{x}|\boldsymbol{\theta})p(\boldsymbol{\theta})] - \mathbb{E}_{q} [\log q_{\lambda}(\boldsymbol{\theta})]) + \log p(\mathbf{x})$$

Second term $\log p(\mathbf{x})$ is constant. The first term $L(\lambda)$ is known as evidence lower bound (ELBO) and by maximising it one can minimise the KL divergence between the variational distribution and the true posterior. So the goal is to solve the following optimization problem:

$$\lambda^* = \underset{\lambda \in \Omega}{\operatorname{arg\,min}} KL(q_{\lambda}(\boldsymbol{\theta})||p(\boldsymbol{\theta}|\mathbf{x})) = \underset{\lambda \in \Omega}{\operatorname{arg\,max}} L(\lambda, \boldsymbol{x}), \tag{4}$$

where Ω is the set of all possible values of the hyperparameters λ . The overall idea is schematically presented in Figure 2. It is assumed that the model parameters are random variables. However, their true distribution is almost always unknown. In such a case, the best option is to select an approximate candidate distribution that will be used instead. Instead of selecting a candidate distribution ad hoc, we try to incorporate prior knowledge as much as possible, in particular the support interval, previous empirical observations, etc. Therefore, it is likely to choose a candidate distribution sufficiently close to the true but unknown parameter's distribution. As some mismatch is usually always present, that causes a bias in the VB solution. However, this is a small price to pay compared to the substantial increase in the computational efficiency of the VB. The VB algorithm was implemented in Python using the PyTorch [30] library. For a link to the implementation and an example data set sufficient to recreate a numerical example, see Appendix A.

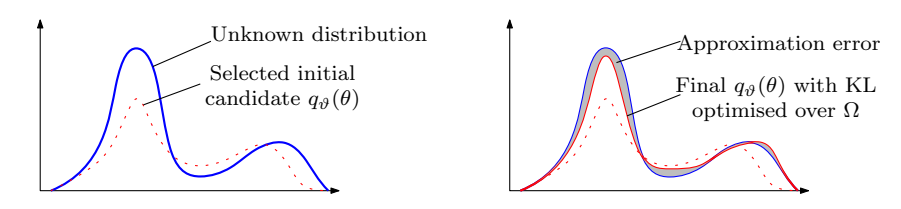


Figure 2: Optimisation process of finding the closest variational distribution $q_{\lambda}(\theta)$ over the set of latent variables λ .

2.3. Finding the optimal hyper-parameters

Using VB we convert the problem of finding the posterior distributions from statistical inference to a much simpler task of optimising a cost function for a variational family parameterised by the vector of hyperparameters λ . The cost function in this case is ELBO. For the optimization part of our algorithm we use the adaptive moment estimation (ADAM) optimizer [31].

ADAM allows an adaptive correction of the learning rates for each element $\lambda^{(s)}, s = 1, ..., \nu$ of the vector λ during the run of the algorithm by calculating the first and second moment of the gradient, denoted as $m_t^{(s)}$ and $v_t^{(s)}$ respectively. This is done using exponentially moving averages computed on the gradient $g_t^{(s)}, s = 1, ..., \nu$

$$m_t^{(s)} = \beta_1 m_{t-1}^{(s)} + (1 - \beta_1) g_t^{(s)}$$

$$v_t^{(s)} = \beta_2 v_{t-1}^{(s)} + (1 - \beta_2) \left(g_t^{(s)} \right)^2,$$
(5)

where t denotes the iteration number and $\beta_{1,2}$ are the parameters of the moving average. The default values for β parameters are 0.9 and 0.999 and the initial values of first and second moment of the gradient are both set to 0, since it turns out this does not impact the convergence rate significantly. For a set of measured data (impedance in our case) x the gradients can be presented with the following vector

$$\boldsymbol{g}_t = \left(g_t^{(1)}, \dots, g_t^{(\nu)}\right)^T = \nabla_{\boldsymbol{\lambda}_t} L(\boldsymbol{\lambda}_t, \boldsymbol{x}).$$
 (6)

First and second moments are only estimated with $m^{(s)}$ and $v^{(s)}$, therefore we want them to satisfy the following condition

$$\mathbb{E}\{m_t^{(s)}\} = \mathbb{E}\left(g_t^{(s)}\right)$$

$$\mathbb{E}\{v_t^{(s)}\} = \mathbb{E}\left((g_t^{(s)})^2\right)$$
(7)

Above conditions ensure that we are dealing with unbiased estimates. First moment at step t in the recursive equation (5) is

$$m_t^{(s)} = (1 - \beta_1) \sum_{i=1}^t \beta_1^{t-i} g_i^{(s)}.$$
 (8)

We can see some bias still occurs in this estimate. Applying expected value operator to equation (8) gives

us

$$E_{\lambda}\left[m_{t}^{(s)}\right] = (1 - \beta_{1}) \sum_{i=1}^{t} \beta_{1}^{t-1} E_{\lambda}\left[g_{i}^{(s)}\right]$$

$$\approx (1 - \beta_{1}) \left(\sum_{i=1}^{t} \beta_{1}^{t-1}\right) E_{\lambda}\left[g_{t}^{(s)}\right]$$

$$= \left(1 - \beta_{1}^{t}\right) E_{\lambda}\left[g_{t}^{(s)}\right].$$

$$(9)$$

Bias correction is done automatically by ADAM during the evaluation of m and v as follows

$$\hat{m}_t^{(s)} = \frac{m_t^{(s)}}{1 - \beta_2^t}$$

$$\hat{v}_t^{(s)} = \frac{v_t^{(s)}}{1 - \beta_2^t}.$$
(10)

Optimisation steps are also adjusted. For each individual parameter the algorithm updates

$$\lambda_t^{(s)} = \lambda_{t-1}^{(s)} - \eta \frac{\hat{m}_t^{(s)}}{\sqrt{\hat{v}_t^{(s)} + \eta}},\tag{11}$$

where $\eta = 0.001$.

The use of ADAM is spreading over a wide range of applications and delivers efficient and fast results. It should be noted, however, that as a heuristic optimization algorithm there is no general guarantee of convergence. Fortunately, Kingma and Ba [31] proved that the algorithm converges globally in the convex settings. This was further refined and proved by Reddi et al. [32]. We used the default settings of $\beta_1 = 0.9$ and $\beta_2 = 0.999$, while setting the learning rate and the number of iterations depending on the data set at hand.

3. Numerical example

Since we focus on solid oxide fuel cells in this paper, we will first demonstrate the performance of VB algorithm using simulated data. A rather frequently used ECM model structure of SOFC takes the following form:

$$Z(\omega) = R_s + \sum_{i=1}^{N} \frac{R_i}{(j\omega)^{\alpha_i} Q_i R_i + 1} + j\omega L$$
(12)

where R_s stands for serial resistance, each pole is defined with the corresponding R_i (parallel resistor) and Q_i (constant-phase element) parameter value, fractional order of i^{th} pole is denoted with $\alpha_i \in (0,1]$ and $\omega = 2\pi f$, where f is the frequency interval. The "true" impedance (12) was simulated on the frequency interval $f \in [10^{-4}, 10^4]$ Hz by using parameters listed in Table 1. For the simulation we used Grünwald-Letnikov approximation for the fractional derivative [33]. G-L fractional derivative is susceptible to noise in the data, therefore the simulation was performed using noiseless signals and measurement noise was added afterwards.

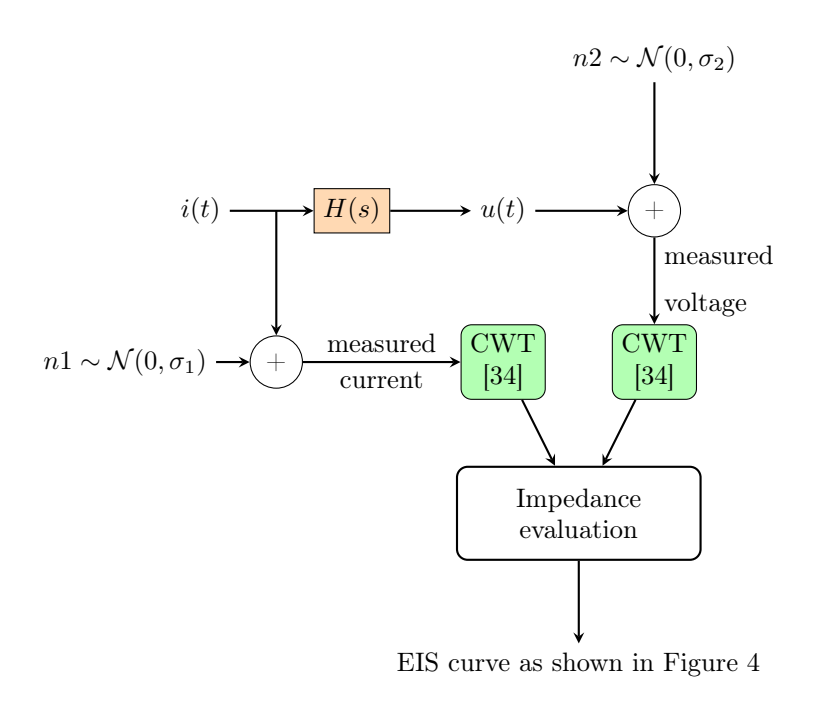


Figure 3: Simulated EIS curve with noisy input and output.

The additive measurement noise was applied separately to the voltage u(t) and current i(t) as $n_1(t)$ and $n_2(t)$ respectively. It should be noted that $n_1(t)$ and $n_2(t)$ are zero-mean and uncorrelated. Having the simulated input and output signals the transfer function was estimated from Morlet wavelet transform of the input and output as described in [34]. The entire process is presented in Figure 3.

The first step in applying the VB approach is the definition of variational distributions that approximate the true posterior $p(\boldsymbol{\theta}|\mathbf{x})$. They are listed in Table 1. For our case $\boldsymbol{\theta} \in \mathbb{R}^{10}_+$, with additional limitation as $\alpha_i \in [0,1]$. Beta distribution was therefore chosen as the best fit for the $\alpha_i, i \in \{1,2,3\}$ parameters and Log-normal distribution for the rest. We selected the means and variances for our variational distributions and then determined their parameters using (13) and (14).

The rough estimates of informative variational distributions can be assessed in an efficient manner from the EIS curve in Figure 4 and previous experience (expert knowledge). In the upper plot in Figure 4 one can notice that the real part of the curve starts around 3 Ω . This provides a rough estimate for the parameter R_s , i.e. selecting variational distribution with mean 2.5 Ω and variance to 1 seems a reasonable choice. The next step is setting the variational distributions for the parameters $R_{1,2,3}$. Just by looking at the axis values, it is apparent that they should be located within the interval (1,10) Ω . Mean values of their distributions were therefore set in the middle of the interval. Variational distributions of the parameters $Q_{1,2,3}$ was roughly estimated by the results of previous experiments and by incorporating experts knowledge. Lastly, the fractional order powers $\alpha_{1,2,3}$ are expected to have values in the interval [0.5,1].

Table 1: Model parameters and variational distributions calculated using equations (13) and (14).

True parameter	Variational distribution
$R_s=3~\Omega$	$\sim \text{Lognormal}(0.84, 0.39)$
$R_1 = 1 \ \Omega, \ R_2 = 2 \ \Omega, \ R_3 = 3 \ \Omega$	$\sim \text{Lognormal}(1.59, 0.20)$
$Q_1 = 0.1 \ Fs^{\alpha_1}$	$\sim \text{Lognormal}(-0.35, 0.83)$
$Q_2 = 5 F s^{\alpha_2}$	$\sim \text{Lognormal}(1.96, 0.83)$
$Q_3 = 150 \ Fs^{\alpha_3}$	$\sim Lognormal(4.99, 0.55)$
$\alpha_1 = 0.88, \alpha_2 = 0.82, \alpha_3 = 0.99$	$\sim \text{Beta}(13.91, 5.68)$
$L = 100 \ nH$	

Once we have determined the mean and variance of our variational distributions, we have to transform them into the correct parameters for the chosen distributions. To obtain the parameters of the lognormal distribution (σ_{ln}, μ_{ln}) from the mean and variance (σ, μ) , the following equations can be used:

$$\sigma_{ln} = \ln\left(\frac{\sigma^2}{\sqrt{\sigma^2 + \mu^2}}\right) \qquad \mu_{ln} = \ln\left(1 + \frac{\mu^2}{\sigma^2}\right)$$
 (13)

and for beta distribution parameters α and β e.g. Beta (α, β) we use:

$$\alpha = \frac{\sigma^2 - \sigma^3}{\mu} - \sigma \qquad \beta = \frac{\alpha}{\sigma} - \alpha \tag{14}$$

The optimization was performed using a global learning rate of 0.05. The optimization was completed after 25000 steps. ELBO loss curve can be observed in Figure 5. By sampling the resulting posterior distributions and simulating the model (12) it is possible to visualize the obtained results. For this purpose, 1000 samples were drawn for each parameter from their respective posterior distribution. Simulating the 1000 EIS curves with the sampled sets of parameters gave us an estimate of the confidence interval of our results, which can be found in Figure 4. The EIS curve obtained from the means of the posterior distributions for the parameters can also be found on the same Figure. The variance of the posterior distributions is effectively presented with the sampled curves and it is bounded by the noise variance parameter. The mean EIS curve seems to be a sufficiently good fit for the input data.

The evolution of the optimization process for each parameter is presented in Figure 6, where we can also find the true parameters used for the simulation of our input data. We can see that each parameter reaches its true value, except Q_3 . We can assume this is the effect of noise, which seems to be greater in the third arc, as seen in Figure 4. Progress in confidence of the algorithm can be easily observed with the help of the evolution of estimated spread in parameters distributions. As seen in the Figure 6, at the beginning the spread is wide and as the optimization progresses and explores larger search space it steadily decreases.

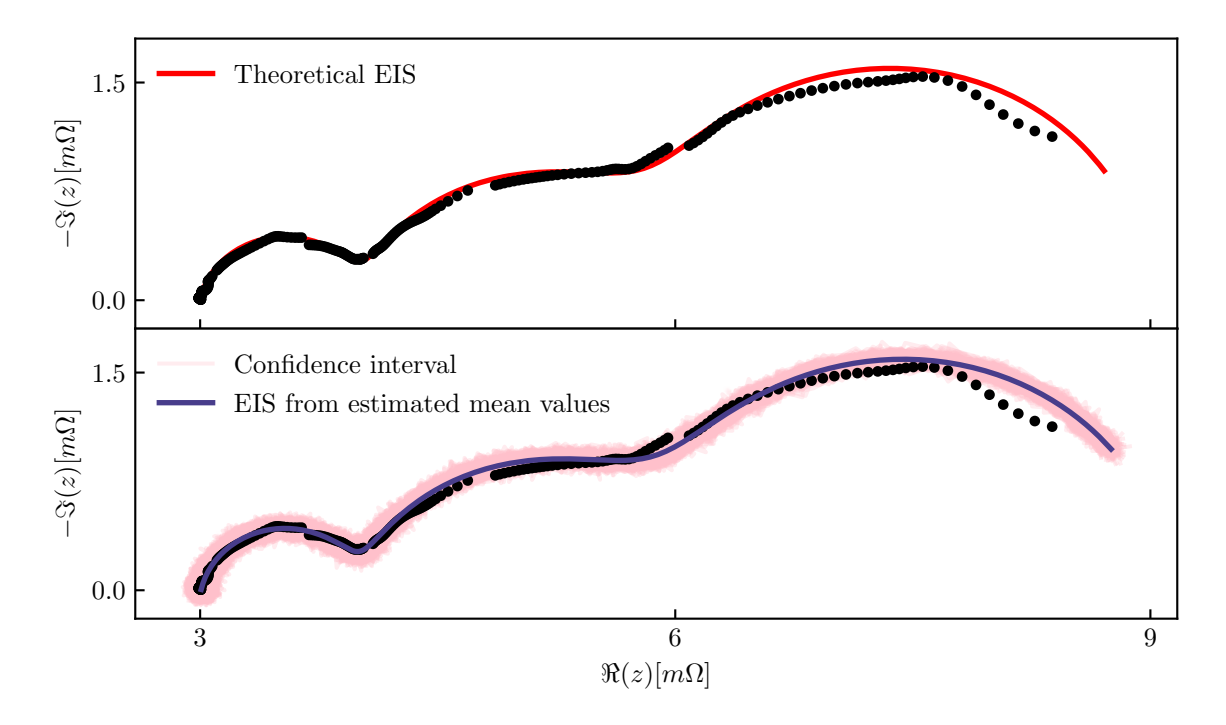


Figure 4: Simulated measurement data (above) and results of the VB algorithm (below).

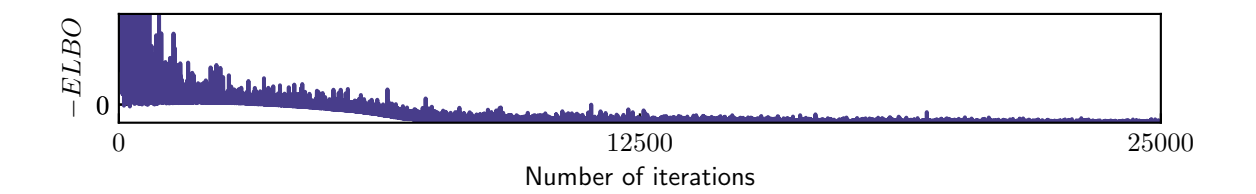


Figure 5: ELBO loss.

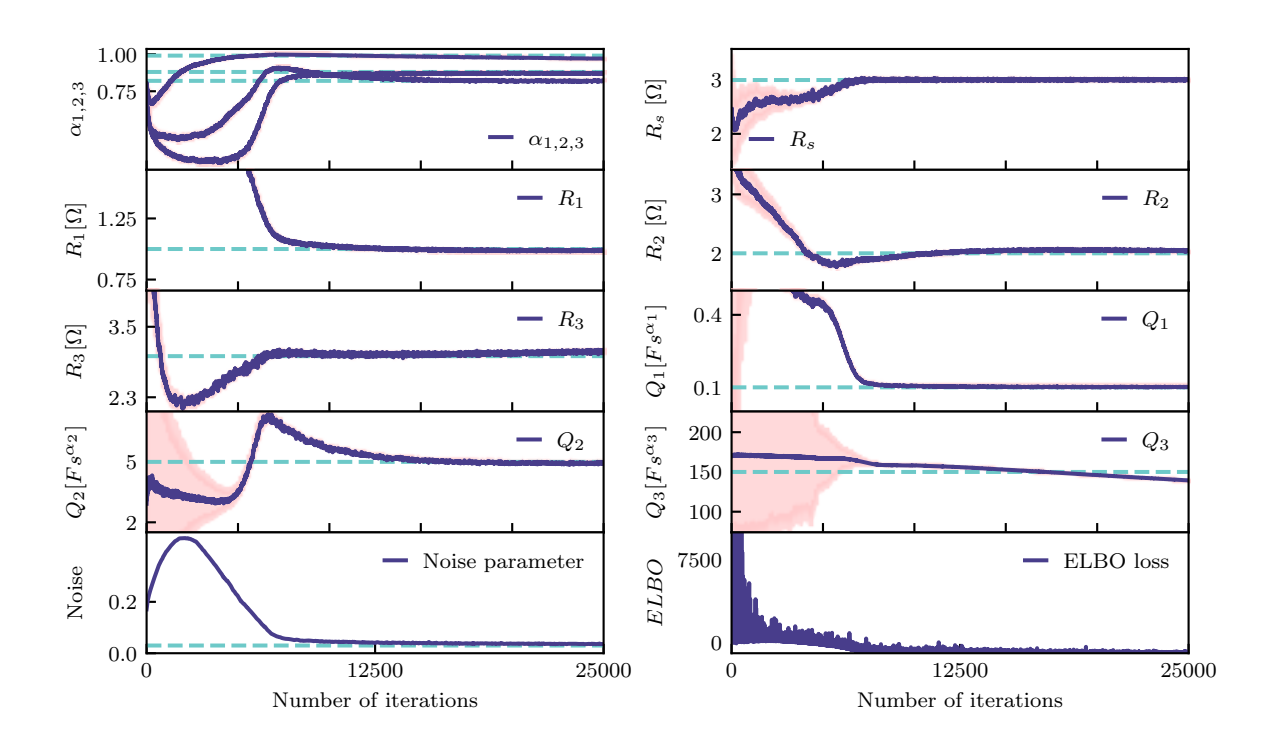


Figure 6: Progress of parameter estimation during the optimisation process, true values of parameters used for simulation are represented with dashed lines. The variance of the estimated distribution(pink) is quite low. The selected optimal shape of the posterior distributions are shown in Figure 7.

The resulting posterior distributions of the model parameters as well as the posteriors obtained with MCMC are shown in Figure 7. Three key observations can be made. First, comparing posterior and variational distributions, the optimisation process was capable of reaching the "true" mean values even for cases when the variational means were "far" from the simulated values. Second, the scales (variance) of the posterior distributions are low, leading to the conclusion that the obtained model has low uncertainty. Table 2 lists all resulting posterior parameter distributions. Third, the empirical posteriors obtained through MCMC method are similar to the ones obtained by VB approach. It should be noted that in some cases VB approach posteriors can be under-dispersed (lower variance) compared with the ones obtained by MCMC. Being overconfident is a well known behavioural trait of VB algorithm and mathematical proofs of this behaviour under certain conditions is provided by Blei and Wang [9, 35]. Our results seem to fit the MCMC results reasonably well, with minor overconfidence in the posterior distributions of $R_{1,2}$ and Q_3 .

Table 2: Posterior distributions of parameters.

$R_s \sim \text{Lognormal}(1.0, 0.0006)$				
$R_1 \sim \text{Lognormal}(-0.011, 0.003)$	$R_2 \sim \text{Lognormal}(0.72, 0.002)$	$R_3 \sim \text{Lognormal}(1.12, 0.003)$		
$Q_1 \sim \text{Lognormal}(-2.28, 0.0007)$	$Q_2 \sim \text{Lognormal}(1.6, 0.007)$	$Q_3 \sim \text{Lognormal}(4.94, 0.004)$		
$\alpha_1 \sim \text{Beta}(969.35, 144.11)$	$\alpha_2 \sim \text{Beta}(1016.18, 225.57)$	$\alpha_3 \sim \text{Beta}(4724.72, 144.39)$		

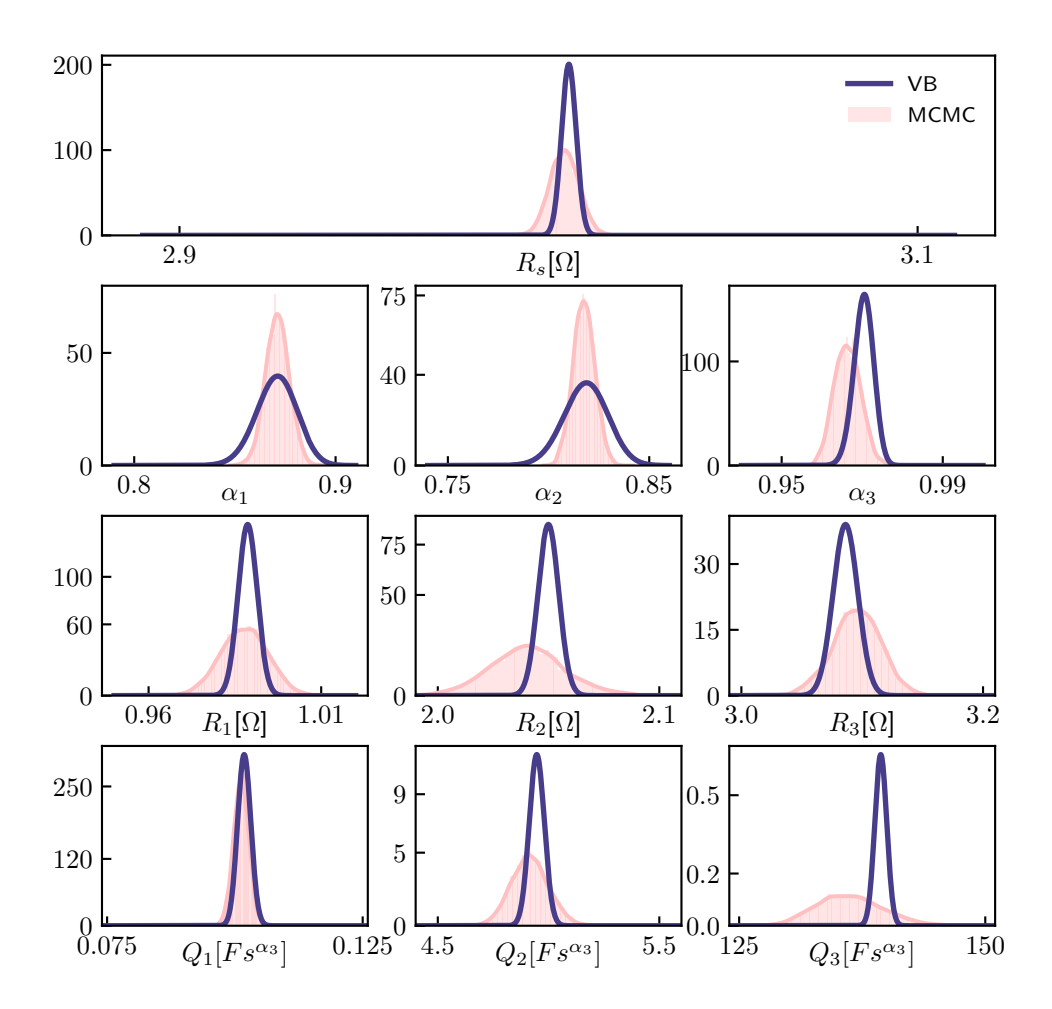


Figure 7: Posterior distributions of parameters derived from simulated data.

4. Experimental validation

The VB was validated using EIS curves measured on anode supported solid oxide fuel cells which were installed in an insulated ceramic housing. The active area of a single cell was 80 cm². The SOFC short stack was fed with a mixture of hydrogen and nitrogen with a flow rate $H_2/N_2=0.216/0.144$ Nl h^{-1} cm⁻² whereas the air flow rate was 4 Nl h^{-1} cm⁻². Stack was operated at nominal current of 32 A (0.4 A cm⁻²) with FU=77.5 %.

The EIS curves were obtained by inducing current excitation (galvanostatic mode) by means of the discrete random binary signal. The excitation current had DC value of I_{DC} =32 A with peak-to-peak amplitude of 2 A. The amplitude was chosen so that it stays in the linearity region, but still big enough to maintain sufficient signal-to-noise ratio.

The current and voltage sensor have sufficiently wide frequency bandwidth with cut-off frequency of 240 kHz. The cell voltages were measured independently using a differential 16-bit NI USB-6215 data acquisition system. The analogue signals were firstly low pass filtered at 10.8 kHz and sampled with sampling frequency $f_s = 50$ kHz.

4.1. Experimental results

The measured EIS curve is shown in Figure 8. Note here that the noise in measurements is quite low thanks to the quality data acquisition equipment and the well controlled laboratory conditions for the experiment. The first step in the identification process is the selection of the model structure, i.e. the number of poles.

It is believed that overall 5 main diffusion processes are going on within the cell. However, some of them are very fast, for example charge transfer and its dynamics is beyond the capability of the available data acquisition systems, whose bandwidth is limited above to cca. 1kHz. Therefore N=3 turns to be an appropriate selection that captures the processes that fall within the frequency band of the DAQ system.

Consequently, the model structure was selected to be as in (12) with N=3. Variational distributions were selected by examining the measured EIS curve. If we look at the Figure 8, we can see that the high frequency part of the real component has values around $3m\Omega$, which will serve as the mean value for the R_s parameter. The scale of its distribution was set quite wide to allow the optimization process to explore wide intervals in the search for the optimum. Variational distributions of $R_{1,2,3}$ parameters can be inferred from the complex and real values our EIS curve takes that their values should be roughly between the interval [0.1,3] m Ω . From previous testing we can assume that with the similar R values and visible poles the $Q_{1,2,3}$ parameters will be at least by an order of 10 apart, so we assumed they are located at 1,50 and 500 Fs^{α_1} respectively. The scales for their variational distributions were set respectively large. Finally, for $\alpha_{1,2,3}$ we can assume from experience that they probably take values between 0.5 and 1.0. All the variational distributions can be seen on Table 3.

Table 3: Variational distributions of parameters.

$R_s \sim \text{Lognormal}(-5.86, 0.32)$	$R_{1,2,3} \sim \text{Lognormal}(-8.41, 1.27)$	$\alpha_{1,2,3} \sim \text{Beta}(12,3)$
$Q_1 \sim \text{Lognormal}(-2.31, 2.14)$	$Q_2 \sim \text{Lognormal}(3.57, 0.83)$	$Q_3 \sim \text{Lognormal}(6.20, 0.20)$

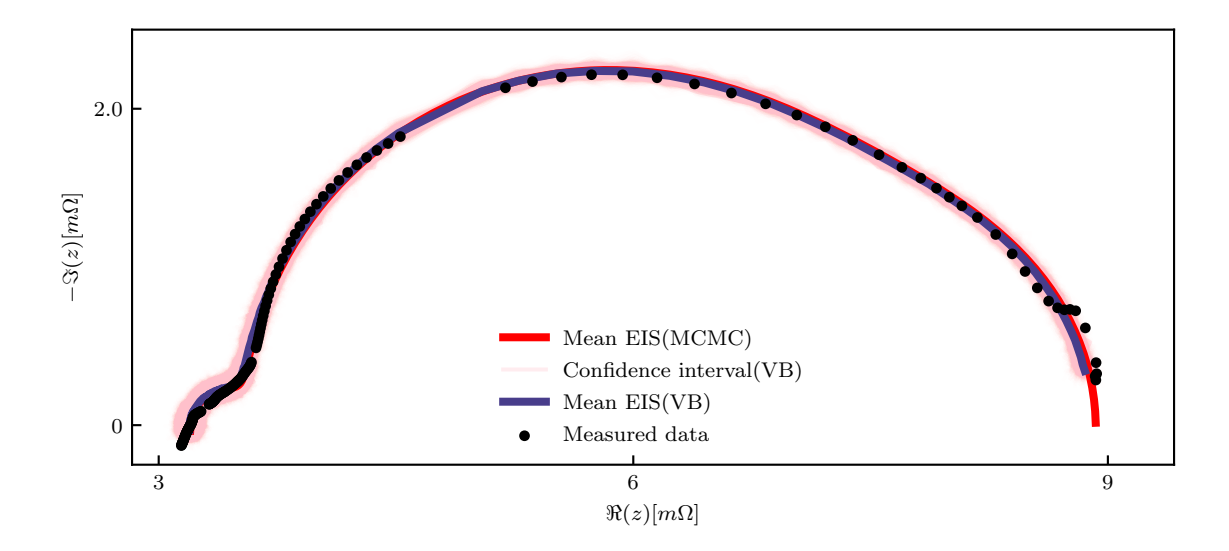


Figure 8: Input measurement data and resulting simulated EIS curves.

The learning rate was set to 0.005. This value is lower than in the numerical example, since the goal was to allow steady and efficient estimation. The optimization finished after 35000 steps.

The performance of the algorithm can best be observed by looking at the EIS curves obtained from the posterior distributions of the estimated parameters. In the same manner as with numerical example, we also took 1000 samples from each of parameters posterior distribution, to simulate 1000 EIS curves. The confidence interval is shown in Figure 8, together with the EIS curve obtained from the posterior means.

The results confirm that despite the low number of iterations, the resulting parameters represent an accurate fit for the measured EIS data.

The evolution of ELBO can be seen in Figure 9. Evidently the plot converges. Comparing with the Figure 5 we can notice that the rate of convergence is slower, which can be associated with the much smaller learning rate and smaller number of iterations used for the run on experimental data. As we approach the end of the computation, the ELBO value changes minimally, which means we have found our optimum for the estimation.

The evolution of parameter estimation is shown in Figure 10. The algorithm steadily converges towards the optimum, while the estimated spread for each parameter continues to narrow. The parameter evolution is very smooth for each parameter. Posterior distributions are shown in Figure 11, where we compare them

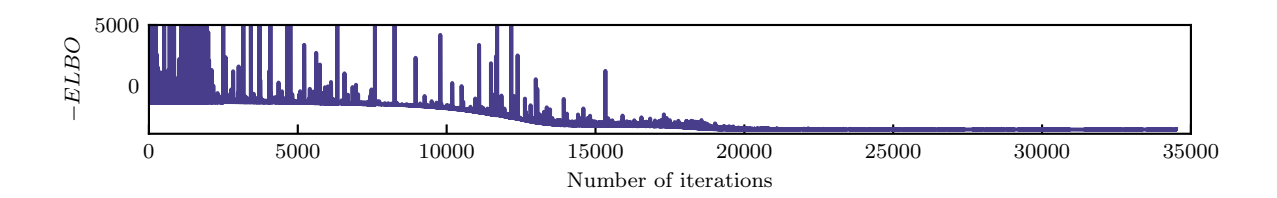


Figure 9: The evolution of ELBO for experimental data.

with results of MCMC algorithm. We can see the expected slight overconfidence of VB, while the results are still inline with MCMC results. It is apparent that scales (variance) of the posterior distributions are quite low. Posterior parameter distributions are listed in Table 4.

Table 4: Posterior distributions of parameters.

	$R_s \sim \text{Lognormal}(-5.75, 8.3e^{-4})$	
$R_1 \sim \text{Lognormal}(-7.995, 0.011)$	$R_2 \sim \text{Lognormal}(-6.33, 0.0039)$	$R_3 \sim \text{Lognormal}(-5.61, 0.0075)$
$Q_1 \sim \text{Lognormal}(2.25, 0.0086)$	$Q_2 \sim \text{Lognormal}(6.22, 0.0025)$	$Q_3 \sim \text{Lognormal}(3.96, 0.0028)$
$\alpha_1 \sim \text{Beta}(1081.56, 41.42)$	$\alpha_2 \sim \text{Beta}(2216.36, 187.46)$	$\alpha_3 \sim \text{Beta}(399.28, 0.495)$

4.2. Discussion

Results in Figure 8 that the ECM identified through the VB approach provide an accurate fit for the measured data

From ELBO plot in Figure 9 it is evident the algorithm converges. The same observation holds true for the estimated parameters, as shown in Figure 10.

Comparing the resulting posterior distributions from both VB and MCMC in Figure 11 we can conclude the following. First, results show close match for every parameter, with only a slight mismatch noticeable in R_S , α_1 and Q_1 . Second, the posterior distributions obtained with VB have lower dispersion (variance) than the ones obtained through MCMC. As mentioned above, this is common for VB approach.

One of the reasons for having overconfident results might be in the selection of the variational distributions. A possible improvement might be achieved by using more elaborated approximations in terms of a mixture of bounded distributions [36]. That is a topic of further research.

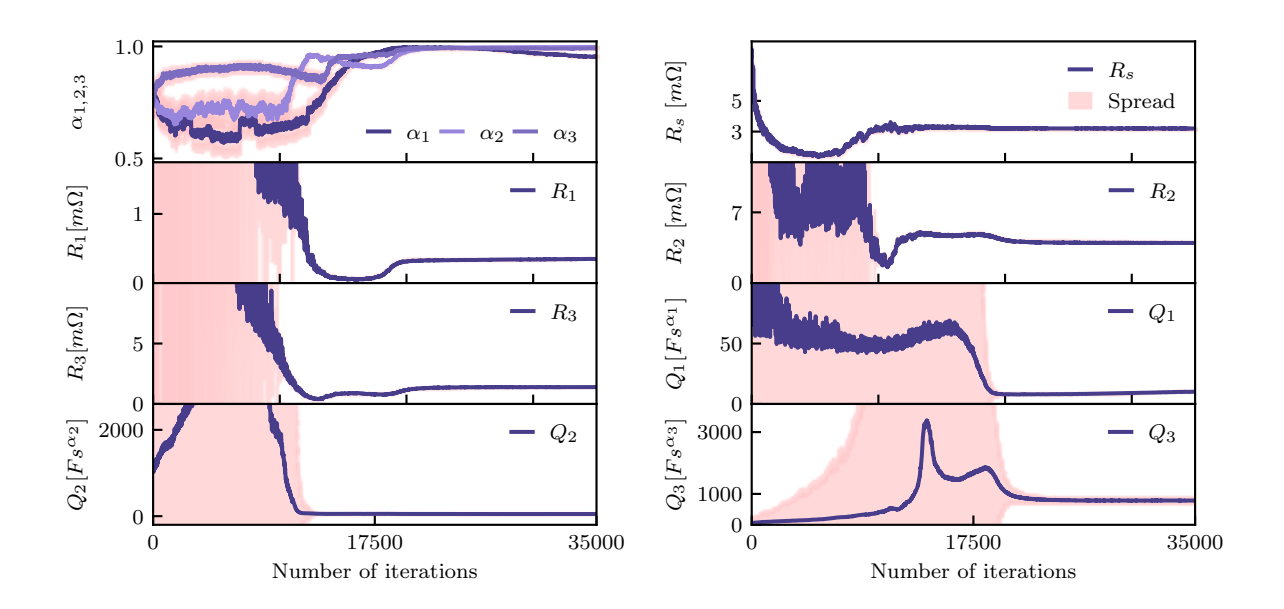


Figure 10: The evolution of parameter estimation for experimental data. Estimated parameter spread at each iteration enveloping the mean of the parameter at given iteration.

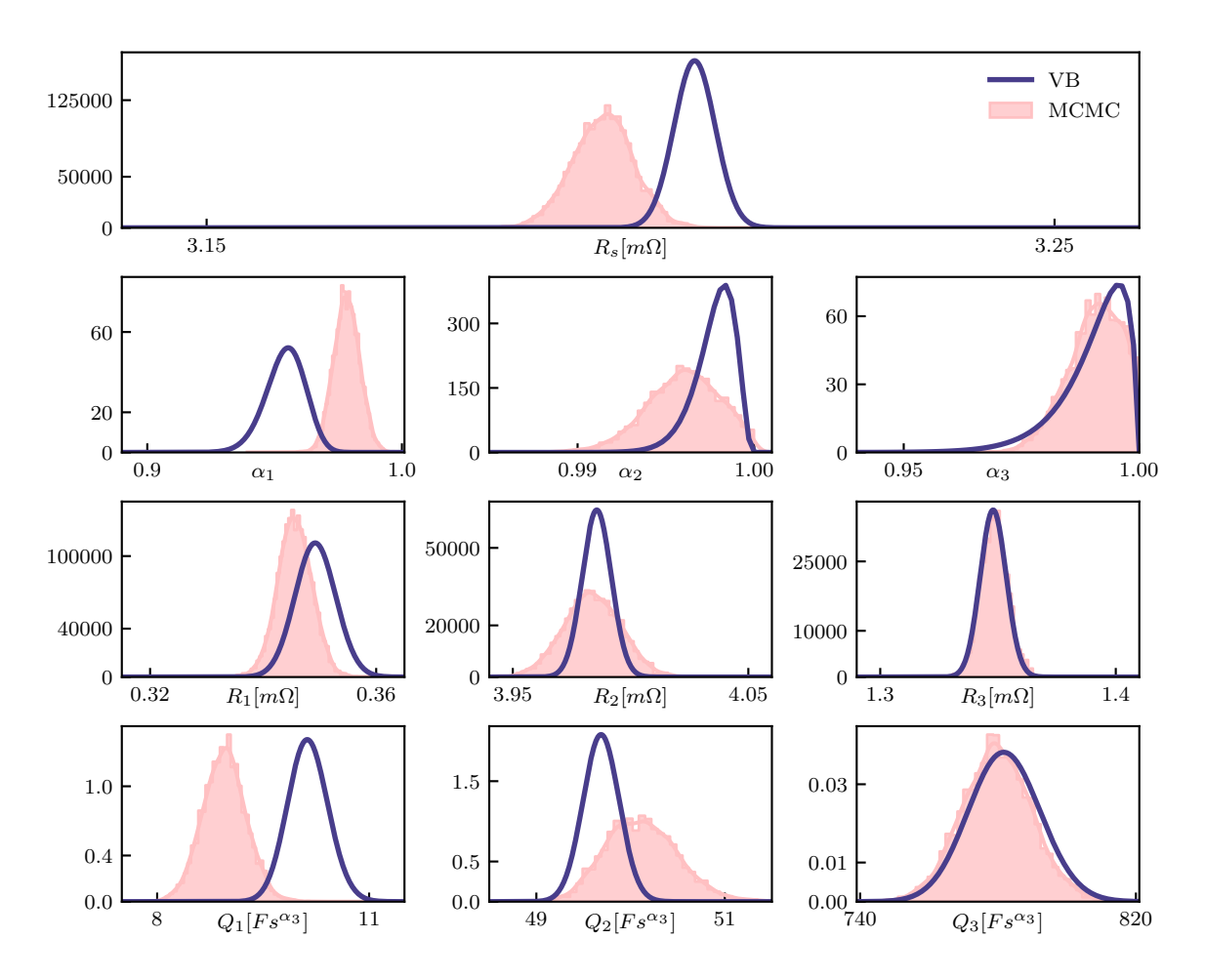


Figure 11: Posterior distributions of parameters inferred with experimental data.

5. Conclusion

The evaluation of the uncertainty of EIS measurements is particularly important for practical applications. The proposed VB approach for ECM parameter estimation provides a solution to this problem. The obtained posterior distributions of ECM model parameters provides a better insight on the condition of the observed fuel cell. As a result, it becomes possible to employ more powerful statistical decision tools for change detection.

The computational load of VB method is far lower than MCMC and the implementation is quite straightforward. The power of VB was shown for the use on SOFC, but it is also possible to apply a similar application for more general parameter estimation problems. This opens the possibility of harnessing the stochastic nature of the model parameters with the goal of applying statistical methods for diagnostics and health prognosis of electrochemical energy systems.

Acknowledgements

The authors acknowledge the support from the Slovenian Research Agency through the programme P2-0001 and project J2-9441. Part of the support is received through the project RUBY (grant agreement No. 875047) within the framework of the Fuel Cells and Hydrogen 2 Joint Undertaking under the European Union's Horizon 2020 research and innovation programme, Hydrogen Europe and Hydrogen Europe research.

References

- [1] A. Lasia, Electrochemical Impedance Spectroscopy and its Applications, Springer-Verlag, New York, 2014.
- [2] V. Subotić, N. H. Menzler, V. Lawlor, Q. Fang, S. Pofahl, P. Harter, H. Schroettner, C. Hochenauer, On the origin of degradation in fuel cells and its fast identification by applying unconventional online-monitoring tools, Applied Energy 277 (2020) 115603. URL: http://www.sciencedirect.com/science/article/pii/S0306261920311107. doi:https://doi. org/10.1016/j.apenergy.2020.115603.
- [3] E. A. Adinolfi, M. Gallo, P. Polverino, D. Beretta, S. S. Araya, C. Pianese, Ecm-based algorithm for on-board pemfcs diagnosis, in: W. Zamboni, G. Petrone (Eds.), ELECTRIMACS 2019, Springer International Publishing, Cham, 2020, pp. 103–115.
- [4] J. Mougin, B. Morel, A. Ploner, P. Caliandro, J. Van Herle, P. Boškoski, B. Dolenc, M. Gallo, P. Polverino, A. Pohjoranta, A. Nieminen, S. Pofahl, J. Ouweltjes, S. Diethelm, A. Leonardi, F. Galiano, C. Tanzi, Monitoring and diagnostics of sofc stacks and systems, ECS Transactions 91 (2019) 731–743. doi:10.1149/09101.0731ecst.
- [5] M. Gallo, P. Polverino, J. Mougin, B. Morel, C. Pianese, Coupling electrochemical impedance spectroscopy and model-based aging estimation for solid oxide fuel cell stacks lifetime prediction, Applied Energy 279 (2020) 115718. URL: http://www.sciencedirect.com/science/article/pii/S0306261920312113. doi:https://doi.org/10.1016/j.apenergy. 2020.115718.
- [6] A. Rakar, Đani Juričić, P. Ballé, Transferable belief model in fault diagnosis, Engineering Applications of Artificial Intelligence 12 (1999) 555 567. URL: http://www.sciencedirect.com/science/article/pii/S0952197699000305. doi:https://doi.org/10.1016/S0952-1976(99)00030-5.

- [7] R. Mosbæk, Solid Oxide Fuel Cell Stack Diagnostics, Ph.D. thesis, 2014.
- [8] A. Leonide, SOFC Modelling and Parameter Identification by Means of Impedance Spectroscopy, Schriften des Instituts für Werkstoffe der Elektrotechnik, Karlsruher Institut für Technologie, KIT Scientific Publ., 2010. URL: https://books.google.si/books?id=kE30tpn2DS8C.
- [9] Y. Wang, D. M. Blei, Variational Bayes under model misspecification, 2019. arXiv:1905.10859.
- [10] P. E. Jacob, S. M. M. Alavi, A. Mahdi, S. J. Payne, D. A. Howey, Bayesian inference in non-markovian state-space models with applications to battery fractional-order systems, IEEE Transactions on Control Systems Technology 26 (2018) 497–506.
- [11] V. Šmídl, A. Quinn, The Variational Bayes Method in Signal Processing, Springer-Verlag, 2006. doi:10.1007/ 3-540-28820-1.
- [12] T. D. Bui, J. Yan, R. E. Turner, A unifying framework for Gaussian process pseudo-point approximations using power expectation propagation (2016). arXiv:1605.07066v3.
- [13] J. Hensman, A. Matthews, Z. Ghahramani, Scalable variational Gaussian process classification (2014). arXiv:1411.2005v1.
- [14] D. J. Rezende, S. Mohamed, D. Wierstra, Stochastic backpropagation and approximate inference in deep generative models (2014). arXiv:1401.4082v3.
- [15] Z. Yang, L. Xie, C. Zhang, Variational Bayesian algorithm for quantized compressed sensing (2012). doi:10.1109/TSP. 2013.2256901. arXiv:1203.4870v2.
- [16] V. P. Oikonomou, S. Nikolopoulos, I. Kompatsiaris, A novel compressive sensing scheme under the variational Bayesian framework, IEEE, 2019, pp. 1–5. doi:10.23919/EUSIPCO.2019.8902704.
- [17] C. Gruhl, B. Sick, Variational Bayesian inference for hidden markov models with multivariate Gaussian output distributions (2016). arXiv:1605.08618v1.
- [18] K. P. Panousis, S. Chatzis, S. Theodoridis, Variational conditional-dependence hidden markov models for human action recognition (2020). arXiv:2002.05809v1.
- [19] S. Levine, Reinforcement learning and control as probabilistic inference: Tutorial and review (2018). arXiv:1805.00909v3.
- [20] Y. Liu, H. Qin, Z. Zhang, S. Pei, Z. Jiang, Z. Feng, J. Zhou, Probabilistic spatiotemporal wind speed forecasting based on a variational Bayesian deep learning model, Applied Energy 260 (2020) 114259. doi:10.1016/j.apenergy.2019.114259.
- [21] Y. Liu, H. Qin, Z. Zhang, S. Pei, C. Wang, X. Yu, Z. Jiang, J. Zhou, Ensemble spatiotemporal forecasting of solar irradiation using variational Bayesian convolutional gate recurrent unit network, Applied Energy 253 (2019) 113596. doi:10.1016/j.apenergy.2019.113596.
- [22] W. Choi, H. Kikumoto, R. Choudhary, R. Ooka, Bayesian inference for thermal response test parameter estimation and uncertainty assessment, Applied Energy 209 (2018) 306-321. doi:10.1016/j.apenergy.2017.10.034.
- [23] W. Choi, K. Menberg, H. Kikumoto, Y. Heo, R. Choudhary, R. Ooka, Bayesian inference of structural error in inverse models of thermal response tests, Applied Energy 228 (2018) 1473–1485. doi:10.1016/j.apenergy.2018.06.147.
- [24] P. Pasquier, D. Marcotte, Robust identification of volumetric heat capacity and analysis of thermal response tests by Bayesian inference with correlated residuals, Applied Energy 261 (2020) 114394. doi:10.1016/j.apenergy.2019.114394.
- [25] B. Dolenc, G. Nusev, P. Boškoski, Bertrand, Morel, J. Mougin, Đani Juričić, Probabilistic deconvolution of solid oxide fuel cell impedance spectra, 2020. doi:10.1007/978-3-030-37161-6.
- [26] M. D. Hoffman, A. Gelman, The no-u-turn sampler: Adaptively setting path lengths in hamiltonian Monte Carlo (????). arXiv:1111.4246.
- [27] J. Salvatier, T. V. Wiecki, C. Fonnesbeck, Probabilistic programming in python using PyMC3, PeerJ Computer Science 2 (2016) e55. URL: https://doi.org/10.7717/peerj-cs.55. doi:10.7717/peerj-cs.55.
- [28] M. Betancourt, A conceptual introduction to Hamiltonian Monte Carlo (????). arXiv:1701.02434.
- [29] D. M. Blei, A. Kucukelbir, J. D. McAuliffe, Variational inference: A review for statisticians (2016). doi:10.1080/01621459.

- 2017.1285773. arXiv:1601.00670v9.
- [30] A. Paszke, S. Gross, F. Massa, A. Lerer, J. Bradbury, G. Chanan, T. Killeen, Z. Lin, N. Gimelshein, L. Antiga, A. Desmaison, A. Kopf, E. Yang, Z. DeVito, M. Raison, A. Tejani, S. Chilamkurthy, B. Steiner, L. Fang, J. Bai, S. Chintala, Pytorch: An imperative style, high-performance deep learning library, in: H. Wallach, H. Larochelle, A. Beygelzimer, F. d'Alché-Buc, E. Fox, R. Garnett (Eds.), Advances in Neural Information Processing Systems 32, Curran Associates, Inc., 2019, pp. 8024-8035. URL: http://papers.neurips.cc/paper/9015-pytorch-an-imperative-style-high-performance-deep-learning-library.pdf.
- [31] D. P. Kingma, J. Ba, Adam: A method for stochastic optimization, 2014. arXiv:1412.6980.
- [32] S. J. Reddi, S. Kale, S. Kumar, On the convergence of adam and beyond (2019). arXiv:1904.09237v1.
- [33] C. Monje, Y. Chen, B. Vinagre, D. Xue, V. Feliu, Fractional Order Systems and Control Fundamentals and Applications, 2010. doi:10.1007/978-1-84996-335-0.
- [34] P. Boškoski, A. Debenjak, B. M. Boshkoska, Fast Electrochemical Impedance Spectroscopy, Springer International Publishing, 2017. doi:10.1007/978-3-319-53390-2.
- [35] Y. Wang, D. M. Blei, Frequentist consistency of variational Bayes, Journal of the American Statistical Association 114 (2018) 1147–1161. URL: http://dx.doi.org/10.1080/01621459.2018.1473776. doi:10.1080/01621459.2018.1473776.
- [36] C. Tenreiro, Boundary kernels for distribution function estimation, REVSTAT Statistical Journal 11 (2013) 169–190.

Appendix A. Supplementary material: numerical implementation

Supplementary material containing numerical implementation of the VB algorithm can be found at https://repo.ijs.si/lznidaric/variational-bayes-supplementary-material. Python Jupyter notebook file SupplementaryMaterialSVI.ipynb contains the main algorithm. Data set used to recreate the results presented in this article can be found in NumPy file dataset.npz. Repository contains all the needed scripts for implementation of VB algorithm. Simulation of data was however done separately, so the code is not included.